Scripta Materialia 229 (2023) 115348

Contents lists available at ScienceDirect

Scripta Materialia

journal homepage: www.journals.elsevier.com/scripta-materialia

Trans-twin dislocations in nanotwinned metals

Linfeng Bu [a,b,1], Zhao Cheng [b,1], Yin Zhang [c], HengAn Wu [a], Ting Zhu [c,*], Lei Lu [b,*]

[a] CAS Key Laboratory of Mechanical Behavior and Design of Materials, Department of Modern Mechanics, CAS Center for Excellence in Complex System Mechanics, University of Science and Technology of China, Hefei 230027, China
[b] Shenyang National Laboratory for Materials Science, Institute of Metal Research, Chinese Academy of Sciences, Shenyang 110016, China
[c] Woodruff School of Mechanical Engineering, Georgia Institute of Technology, Atlanta, GA 30332, USA

ARTICLE INFO

Keywords:
Nanotwinned Cu
Trans-twin dislocation
Molecular dynamics
Threading dislocation
Effective stress

ABSTRACT

The strength-controlling dislocation mechanism of a material can be illuminated by partition of the flow stress into its effective stress and back stress components. Recent experiments report a nearly constant saturated effective stress of about 100 MPa for nanotwinned Cu with a range of nanotwin thicknesses less than 100 nm [*Z. Cheng et.al., Proc. Natl. Acad. Sci. U.S.A. 119 (2022) e2116808119*]. This surprising result implies that the effective stress is controlled by the long dislocations spanning multiple nanotwin lamellae, termed trans-twin dislocations, rather than the commonly thought threading dislocations confined within individual nanotwin lamellae. Here we use molecular dynamics to simulate the formation and motion of trans-twin dislocations across multiple nanotwin lamellae. We show that the interconnected segments of a trans-twin dislocation can glide concertedly on the corrugated {111} slip planes in consecutive nanotwin lamellae with little resistance from coherent twin boundaries. Our results indicate that the finite resistance to slip transmission across coherent twin boundaries can set a lower limit of the effective obstacle spacing to hinder dislocation glide and thus dictate the upper limit of the saturated effective stress of nanotwinned metals. This work provides new understanding of the strength-controlling mechanism in nanotwinned metals.

Nanotwinned (NT) metals have been extensively studied for ultra-high strength [1,2], excellent ductility [1,3], extraordinary work hardening [3,4], and enhanced fatigue and fracture resistance [5–8]. These unusual mechanical properties are thought to be controlled by the intra-twin dislocations confined within individual nanotwin lamellae [9–11]. Various experimental and modeling approaches including transmission electron microscopy (TEM) and molecular dynamics (MD) simulation have been used to characterize the interactions between intra-twin dislocations and coherent twin boundaries (CTBs), including the obstruction, transmission, and storage of dislocations by CTBs [12–17]. However, the applied loads in these studies are usually high compared to typical laboratory experiments for bulk NT samples. While these studies have revealed various modes of dislocation-obstacle interactions, it remains largely uncertain regarding the strength-controlling mechanism in NT metals.

Partition of the flow stress into its effective and back stress components can provide important information on the strength-controlling mechanism that often involves dislocation-obstacle interactions in a material. This is because the non-directional effective stress is usually controlled by short-range dislocation-obstacle interactions, while the directional back stress is dictated by long-range dislocation-obstacle interactions [18–20]. The effective stress and back stress can be quantitatively determined from the unload branch of a uniaxial tensile stress-strain curve, and they evolve with applied loading [21]. Recent experiments of NT Cu with preferentially oriented nanotwins showed that the effective stress becomes saturated unexpectedly at about 100 MPa for a range of twin thicknesses from 29 nm to 72 nm, when the tensile loading direction is parallel to CTBs [22]. Since the effective stress is usually controlled by the distance between dislocation pinning obstacles [18], the saturated effective stress of about 100 MPa corresponds to the characteristic obstacle distance of about 300 nm, which is larger than the nanotwin thicknesses less than 100 nm in the NT Cu specimens tested. For this analysis, the Taylor factor of 3.1 is used to convert an applied tensile stress to a resolved shear stress on the primary dislocation slip system [23,24]. Hence, these unexpected results indicate that the effective stress should be controlled by the long dislocations spanning multiple nanotwin lamellae, termed trans-twin dislocations, rather than the commonly thought threading dislocations confined

* Corresponding authors.
E-mail addresses: ting.zhu@me.gatech.edu (T. Zhu), llu@imr.ac.cn (L. Lu).
[1] These authors contributed equally to this work.

https://doi.org/10.1016/j.scriptamat.2023.115348
Received 23 November 2022; Received in revised form 2 February 2023; Accepted 5 February 2023
1359-6462/© 2023 Acta Materialia Inc. Published by Elsevier Ltd. All rights reserved.

within single nanotwin lamellae [23,25]. As schematically illustrated in Fig. 1a, a trans-twin dislocation lies on the corrugated {111} slip planes inclined to CTBs. The interconnected segments of such a trans-twin dislocation share a common Burgers vector parallel to the intersection lines between the corrugated {111} slip planes and CTBs. Hence, these segments are expected to move concertedly with little glide resistance from CTBs, except that the two ends of a trans-twin dislocation are confined by the bounding CTBs.

Direct experimental observation of trans-twin dislocations by TEM remains a challenge. This is because a long trans-twin dislocation line lies on the corrugated {111} slip planes in consecutive nanotwin layers having alternate crystallographic orientations relative to a fixed laboratory frame. As a result, the entire dislocation line cannot be imaged simultaneously under the commonly used dual-beam TEM diffraction condition [13,26], which can only display dislocation line segments in alternate nanotwin layers. On the other hand, MD simulations have revealed the trans-twin dislocations under some special conditions, such as highly refined nanotwins with thicknesses less than 5 nm [27], near a crack tip [28] or in a fatigue sample [29]. However, the crucial role of trans-twin dislocations in controlling the strength of NT metals remain largely unexplored.

In this work, we performed MD simulations to investigate the structure and motion of trans-twin dislocations in NT Cu under applied loading. In MD simulations, we either apply high loads to dislocation-free NT Cu for studying the formation and glide of trans-twin dislocations or embed an individual trans-twin dislocation for studying its responses under controlled loading conditions. These MD simulations provide new understanding of the critical role of trans-twin dislocations in controlling the mechanical properties of NT metals.

Our MD simulations show the formation and expansion of trans-twin dislocations in NT Cu. In Fig. 1b, an as-built sample consists of four columnar grains with a <111> texture normal to the twin plane and a mean grain size of around 40 nm. The four grains have the respective rotation of 0°, 30°, 60° and 90° with respect to the z axis, such that most GBs are of the asymmetrical, high-angle tilt type. Each grain consists of four nanotwin lamellae with the same twin thickness to mimic homogeneous NT Cu. Four types of samples are studied with the respective twin thickness λ of 5.01 nm, 6.26 nm, 9.39 nm to 12.5 nm. The smallest and largest sample contain 11.1 million and 27.5 million atoms, respectively. Each sample is initially equilibrated at 300 K and zero pressure for 250 ps. Then it is subjected to a uniaxial tensile load along the x direction at an applied strain rate of 2×10^8 s^{-1}, while maintaining zero tractions along the transverse y and z directions by using a NPT ensemble [30]. Periodic boundary conditions are imposed in all three directions. The embedded atom method potential of Cu [31] is used. The MD timestep is 1 fs. The common neighbor analysis (CNA) is adopted to display defects. Correspondingly, atoms are colored in green, red and gray to represent the local face-centered cubic (fcc), hexagonal close-packed (hcp) and other structure, respectively. In addition, a position-based coloring scheme is used to enhance the visual effect of dislocation configurations, such that the color of atoms at the dissociated dislocation core vary from orange in the central region of the simulation supercell to green in the boundary region [23].

Fig. 1c shows the MD results of tensile stress-strain curves for the four types of NT Cu samples with different twin thicknesses. Each sample starts with a dislocation-free structure and thus exhibits an initial linear elastic response. Then a maximum stress (up to ~3 GPa) is reached with a subsequent sharp stress drop. The stress drop occurs due to the simultaneous formation of a number of dislocations, resulting in a drastic release of elastic energy. This is followed by the continued generation, motion and annihilation of dislocations. As a result, the flow stress gradually increases, accompanied with large fluctuations due to the relatively small samples used for MD simulations. The average flow stress decreases with increasing twin thickness, which is consistent with the experimental results [23].

Fig. 1d shows the typical dislocation configurations in a sample (λ =

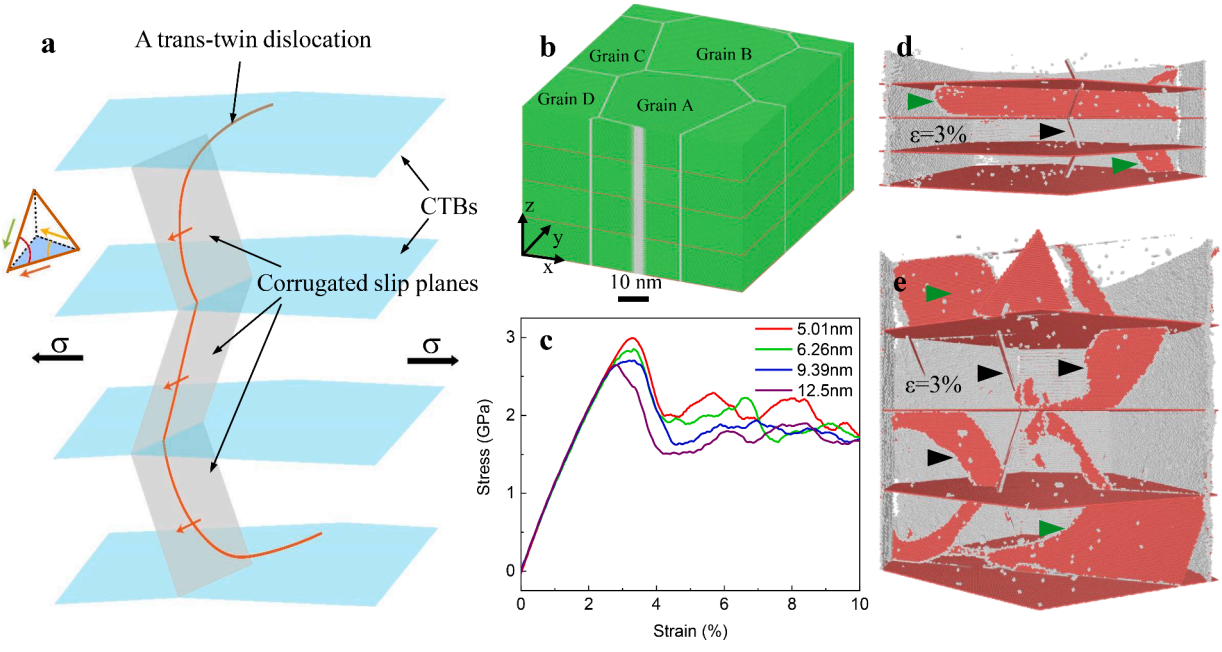

Fig. 1. MD simulations of formation and expansion of trans-twin dislocations. (a) Schematic of an operating trans-twin dislocation on the corrugated {111} slip planes inclined to CTBs, when the NT sample is subjected to a tensile stress σ parallel to CTBs. The orange arrow indicates the Burgers vector of this trans-twin dislocation and the corresponding slip plane is marked as an orange triangle on a reference Thompson tetrahedron. (b) Atomic configuration of a NT Cu sample under tension. Periodic boundary conditions are used and each columnar grain is labeled. The x, y, z axes within grain A are oriented in the crystallographic directions $[\bar{1}01]$, $[1\bar{2}1]$ and [111], respectively. Grains B, C and D are rotated counter-clockwise along the [111] direction (z axis) by 30°, 60° and 90 °, respectively. Green, red and grey colors represent fcc, hcp and disordered atoms, respectively. (c) Stress-strain curves of four NT Cu samples for tension along the x direction. The dislocation configurations are revealed in the NT Cu sample with (d) λ=5.01 nm and (e) λ=12.5 nm at ε = 3%, respectively. Threading dislocations are indicated by green arrowheads and trans-twin dislocations by black arrowheads.

5.01 nm) at an applied tensile strain $\varepsilon = 3\%$. Two types of dislocation configuration are observed. One type is the threading dislocations (indicated by green arrow heads) confined within single nanotwin layers. Each threading dislocation consists of a curved leading partial (gray atoms) followed by a stacking fault ribbon (red hcp atoms). The leading partial nucleates from a GB and then it glides through the grain interior while being confined to a single nanotwin layer. As the leading partial glides forward, its upper and lower edges are bounded by CTBs.

Another type of dislocation configuration is the trans-twin dislocations. As seen from a typical trans-twin dislocation marked by a black arrow head in Fig. 1d, it consists of interconnected segments spanning multiple twin lamellae. This trans-twin dislocation is fully formed and thus has both leading and trailing partials with a short stacking fault ribbon in between. It exhibits a zigzag shape, which arises because its constituent segments lie on the corrugated {111} slip planes with alternate crystallographic orientations in consecutive twin lamellae. As the trans-twin dislocation glides forward under applied loading, a long screw tail is formed along each of the two bounding CTBs. This type of trans-twin dislocations is also observed in other deformed NT Cu samples, such as those marked by black arrow heads in a NT sample with $\lambda =$ 12.5 nm and at $\varepsilon = 3\%$ (Fig. 1e). To mimic the non-uniform distribution of twin thickness in experiments, we also performed MD simulations for NT Cu samples with six nanotwin layers with different λ values from 1.25 to 7.51 nm as well as with tilted CTBs (~5° deviation from the x-y plane). Similar trans-twin dislocations are also observed (Fig. S1). These results demonstrate that the trans-twin dislocations can commonly form in NT Cu regardless of twin thickness.

The fraction of trans-twin dislocations among all the dislocations observed was estimated by counting the trans-twin dislocations and intra-twin dislocations manually. The estimated fractions of trans-twin dislocations are about 60% and 50% at an applied strain $\varepsilon = 4\%$ for the NT Cu sample with twin thickness $\lambda = 5.01$ nm and $\lambda = 12.5$ nm, respectively. These results indicate that the twin thickness does not have a very strong effect on the population of trans-twin dislocations.

The dynamic processes of formation and expansion of trans-twin dislocations are revealed by MD simulations (Fig. 2, Movie S1 and S2). As seen from a NT Cu sample with $\lambda = 9.39$ nm, the leading partial of a threading dislocation first nucleates from the GB (Fig. 2a), and then the trailing partial emerges from the GB (Fig. 2b). As this trailing partial expands in the nanotwin layer, the threading dislocation transmits across one of the two bounding CTBs (Fig. 2b), resulting in two interconnected trans-twin dislocation segments. As the trans-twin dislocation glides forward, slip transmission occurs again across the other bounding CTB, adding one more trans-twin dislocation segment (Fig. 2c, e). Sometimes, two short trans-twin dislocations merge to become one long trans-twin dislocation across a number of nanotwin layers.

The trans-twin dislocations can form two different types of intersection segments at the CTBs, as shown in a NT sample with $\lambda = 12.5$ nm (Fig. 3). For one type of intersection segments (Fig. 3a), each of the two dislocation segments in neighboring nanotwin layers is dissociated into the leading and trailing partials within each layer involved, but constricted to form a very short intersection segment (indicated by black arrow heads) at the CTB. This type of intersection segment results from expansion of the same trans-twin dislocation across multiple nanotwin layers. In neighboring nanotwin layers, the two dislocation segments on the corrugated {111} planes share a common intersection line at the CTB, resulting in the formation of a short intersection segment. For the other type of intersection segments (Fig. 3b), the two dislocation segments in neighboring nanotwin layers are indirectly connected through a relatively long dislocation segment (indicated by black arrow heads)

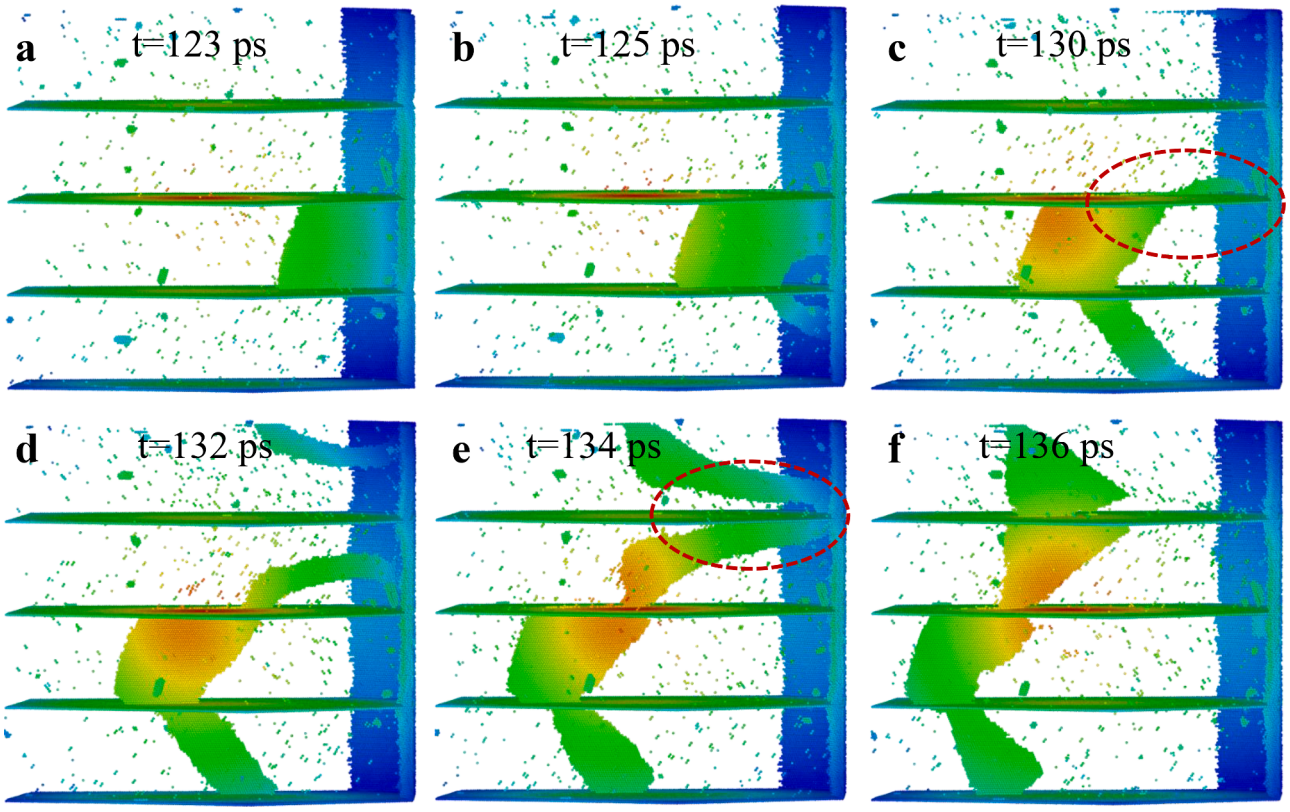

Fig. 2. Dynamic processes of formation and expansion of trans-twin dislocations. (a) The leading partial of a threading dislocation nucleates from the grain boundary. (b) Formation and expansion of a trailing partial in the nanotwin layer leads to slip transmission of the threading dislocation across one of the two bounding CTBs, resulting in two interconnected trans-twin dislocation segments. The dislocation structures (c) before and (d) after the cross-slip of screw tails. The dislocation structures (e) before and (f) after the merging of two trans-twin dislocations. Atoms are colored based on a position-dependent scheme. The red dashed circles indicate the local dislocation configuration before cross-slip.

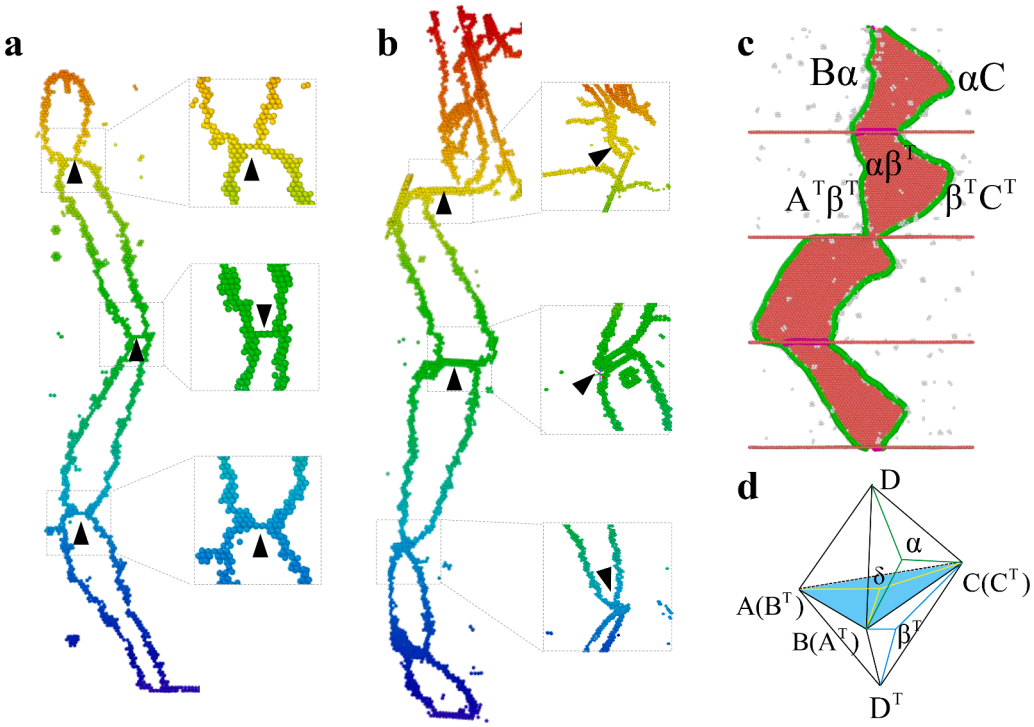

Fig. 3. Trans-twin dislocations form different types of intersection segments at CTBs, as shown in a NT Cu sample with λ=12.5 nm. (a) Extended segments of a trans-twin dislocation are interconnected by short intersection segments (indicated by black arrow heads) at CTBs. (b) Extended segments of another trans-twin dislocation are interconnected by long intersection segments (indicated by black arrow heads). Each intersection segment lies within CTBs and dissociates into the leading and trailing partials as well. (c) The Burgers vectors of a long intersection segment observed in a NT Cu sample with λ=9.39 nm. The green and pink lines represent Shockley partials and stair-rod dislocations, respectively. (d) Double Thompson tetrahedra of the slip systems in two consecutive twin lamellae.

within the CTB, which dissociates into the leading and trailing partials as well. This type of intersection segments results from a linking process between the two trans-twin dislocations, which lie on different sets of corrugated {111} planes in neighboring nanotwin layers that do not share a common intersection line at the CTB. Hence, the screw tail of each of the two neighboring dislocation segments crosses slip into the same CTB, and then the two cross-slipped segments merge into a single intersection segment on the CTB. This type of trans-twin dislocations was observed in previous MD simulations of NT Cu and referred to as correlated necklace dislocations [29].

The two types of intersection segments at the CTBs involve two different types of dislocations, as shown in Fig. 3c for a NT Cu sample with $\lambda = 9.39$ nm. The Burgers vectors of the two types of intersection segments are identified by OVITO [32]. Referring to the double Thompson tetrahedron representing the slip planes in two neighboring nanotwin layers in Fig. 3d, the interconnected dislocation segments in two neighboring twin layers dissociate into partial dislocations **Bα** and **αC**, $\mathbf{A^T\beta^T}$ and $\mathbf{\beta^TC^T}$, respectively. The short intersection segment at the CTB is a dislocation $\mathbf{\alpha\beta^T}$ formed by the reaction between **Bα** and $\mathbf{A^T\beta^T}$. For the relatively long intersection segment in the CTB, the two cross-slipped screw tails in the CTB first dissociate into partial dislocations **Bδ** and **δC**, and merge into a single tail [29]; then **Bα** reacts with **Bδ** to form another stair-rod dislocation **αδ**. Thus, the loop is composed of four dislocation segments, **Bα, αδ, αC** and **δα**. It should be noted that the Burgers vectors of these intersection segments on CTBs are parallel to the intersection lines between the corrugated {111} slip planes and CTBs. Hence, these intersection segments can move concertedly with the interconnected dislocation segments in nanotwin lamellae with little glide resistance from CTBs.

Fig. 4 shows the MD results of gliding of individual trans-twin

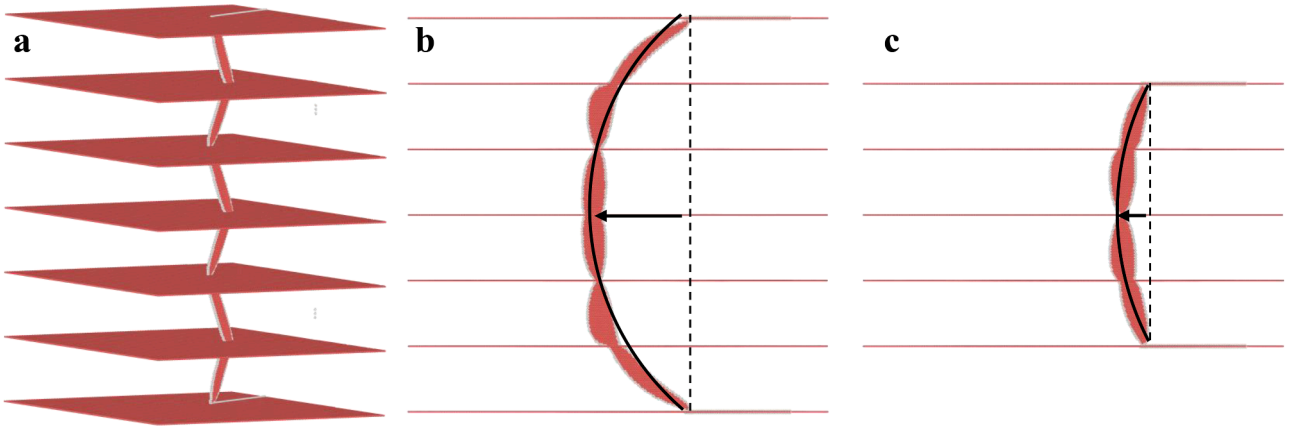

Fig. 4. MD results of a single trans-twin dislocation under applied loading. (a) 3D view of a trans-twin dislocation on the corrugated {111} slip planes inclined to CTBs in a NT sample (λ = 10 nm) without applied loading. (b) The equilibrium configuration of a trans-twin dislocation spanning six twin layers under an applied load of 1GPa when its two ends are fixed to mimic strong pinning obstacles. The atomic structure is viewed along the $[1\bar{2}1]$ direction. The dashed line and solid line outline the configurations of the trans-twin dislocation before and after loading, respectively. (c) Same as (b), except for a trans-twin dislocation spanning four twin layers.

dislocations in an otherwise perfect NT Cu sample with $\lambda = 10$ nm. The use of an initially perfect sample enables the controlled MD simulation of a single trans-twin dislocation under applied loading without interference from other coexisting dislocations. Fig. 4a shows a trans-twin dislocation spanning six twin layers. Its two ends are fixed to mimic strong pinning obstacles. Under an applied tensile stress of 1 GPa, the trans-twin dislocation bows out substantially (Fig. 4b). In contrast, a similar trans-twin dislocation spanning four twin lamellae is only bent slightly (Fig. 4c) under the same applied load. Such different responses demonstrate that for a trans-twin dislocation across less numbers of nanotwin lamellae, a higher driving stress is needed to produce the same extent of bow-out. However, the higher stress applied can provide a stronger driving force for slip transmission of a trans-twin dislocation across CTBs.

The above MD results indicate that the bowing of a trans-twin dislocation across multiple nanotwin layers can be much easier than that of a threading dislocation within a single nanotwin layer. As the applied stress is increased gradually in a NT Cu experiment under a low strain rate (typically less than 10^{-4}/s), the stress needed for moving trans-twin dislocations will be first attained before that of threading dislocations. Continued operation of trans-twin dislocations limits the stress increase in NT Cu, so that the threading dislocations can be hardly moved. In other words, the high stress needed for the operation of threading dislocations is not usually accessible in experiments of NT Cu, while they can be achieved in MD simulations under extremely high strain rates (more than 10^9/s). For the commonly studied NT Cu thin film samples in the literature, the applied tensile load is parallel to CTBs, resulting in large resolved shear stresses for driving the glide of trans-twin dislocations in the corrugated slip planes inclined to CTBs. Hence, the trans-twin dislocations can play a predominant role in the plastic deformation of NT Cu.

We note that when a NT Cu sample is free of trans-twin dislocations like the model used in MD simulation, the initial plastic deformation is controlled by dislocation nucleation (Fig. 2a and b), which is triggered by a high stress up to ~3 GPa. In contrast, a NT Cu sample used in laboratory experiment could contain trans-twin dislocations and easy dislocation sources that are introduced inevitably during sample fabrication. The stress driving the glide of trans-twin dislocations should be much lower than the nucleation stress of trans-twin dislocations. Hence, the dislocation processes that control the effective stress likely correspond to the glide and cross-cutting of trans-twin dislocations rather than the nucleation of trans-twin dislocations.

To understand the relationship between the saturated effective stress and the predominant operation of trans-twin dislocations in NT Cu, we first consider a general limit of the effective stress controlled by dislocation-obstacle interaction. As noted in the Introduction, the effective stress is usually controlled by dislocation-obstacle interaction, and a constant saturated effective stress (e.g., 100 MPa) for a range of nanotwin thicknesses implies a lower limit of the effective obstacle spacing (e.g., 300 nm). In other words, if the effective obstacle spacing were to be smaller than the aforementioned lower limit, the bowing of a dislocation across two pinning obstacles would require a higher driving stress to exert a higher local shear stress on the pinning obstacles. Most obstacles have finite shear strengths, so that they cannot resist against dislocation depinning when the obstacle spacing is smaller than a critical value [33]. Hence, the lower limit of the effective obstacle spacing and the corresponding saturated effective stress are dictated by the finite shear strength of pinning obstacles.

Based on the above analysis of dislocation-obstacle interaction, we can provide a plausible explanation why the saturated effective stress of about 100 MPa from experimental measurements of NT Cu might be controlled by the trans-twin dislocations across multiple nanotwin layers with the combined thickness greater than 100 nm. In the commonly studied NT Cu thin film samples, the external load is mostly applied parallel to CTBs. Under these conditions, the CTBs act as a major type of obstacles to hinder the bowing of a trans-twin dislocation across multiple nanotwin layers. Each CTB has a finite resistance to slip transmission of a screw tail of a bowing trans-twin dislocation [34]. Such resistance should be an almost constant intrinsic property of the CTB. However, if the total thickness of multiple nanotwin layers is smaller than a lower limit, the applied shear stress required to bow out the trans-twin dislocation can become larger than the CTB resistance to slip transmission. As a result, the screw tail of the bowing trans-twin dislocation will transmit across the CTB, resulting in a loss of constraint of the trans-twin dislocation and thus setting an upper limit of the effective stress.

In summary, we have studied a class of trans-twin dislocations in NT metals. Our MD results demonstrate that the bowing of trans-twin dislocations across multiple nanotwin layers can be much easier than that of threading dislocations within individual nanotwin layers. Since the applied stress is gradually increased in typical experiments, the trans-twin dislocations (as coined in this work) rather than the commonly studied threading dislocations can operate favorably and thus play a predominant role during plastic deformation of bulk NT metals. The favorable operation of trans-twin dislocations implies that the saturated effective stress of NT metals is unlikely controlled by the nanotwin thickness less than a lower limit (~300 nm for NT Cu). Hence, there should exist a lower limit of the combined thickness of multiple nanotwin layers for the bowing of trans-twin dislocations, which determines the upper limit of the effective stress of NT metals. The quantitative values of these limits and associated atomic processes warrant further study for different NT metals in the future, thereby enabling a deeper understanding of the strength-controlling dislocation mechanism in NT metals.

Declaration of Competing Interest

The authors declare that they have no known competing financial interests or personal relationships that could have appeared to influence the work reported in this paper.

Acknowledgements

L.L. acknowledge financial support from the National Natural Science Foundation of China (NSFC, Grant Number. 51931010, 92163202), and the Key Research Program of Frontier Science and International partnership program (GJHZ2029), Z.C. acknowledges financial support from National Natural Science Foundation of China (NSFC, Grant Number. 52001312) and the IMR Innovation Fund (Grant Number. 2021-PY02). T.Z. acknowledges financial support from the US National Science Foundation (DMR-1810720).

Supplementary materials

Supplementary material associated with this article can be found, in the online version, at doi:10.1016/j.scriptamat.2023.115348.

References

[1] L. Lu, Y. Shen, X. Chen, L. Qian, K. Lu, Ultrahigh strength and high electrical conductivity in copper, Science 304 (5669) (2004) 422.
[2] X. Zhang, A. Misra, H. Wang, T.D. Shen, M. Nastasi, T.E. Mitchell, J.P. Hirth, R. G. Hoagland, J.D. Embury, Enhanced hardening in Cu/330 stainless steel multilayers by nanoscale twinning, Acta Mater. 52 (4) (2004) 995–1002.
[3] L. Lu, X. Chen, X. Huang, K. Lu, Revealing the maximum strength in nanotwinned copper, Science 323 (5914) (2009) 607–610.
[4] S. Narayanan, G. Cheng, Z. Zeng, Y. Zhu, T. Zhu, Strain hardening and size effect in five-fold twinned Ag nanowires, Nano Lett. 15 (6) (2015) 4037–4044.
[5] A. Singh, L. Tang, M. Dao, L. Lu, S. Suresh, Fracture toughness and fatigue crack growth characteristics of nanotwinned copper, Acta Mater. 59 (6) (2011) 2437–2446.
[6] A.M. Hodge, T.A. Furnish, A.A. Navid, T.W. Barbee, Shear band formation and ductility in nanotwinned Cu, Scr. Mater. 65 (11) (2011) 1006–1009.
[7] S.W. Kim, X. Li, H. Gao, S. Kumar, *In situ* observations of crack arrest and bridging by nanoscale twins in copper thin films, Acta Mater. 60 (6) (2012) 2959–2972.

[8] H.Z. Zhao, Z.S. You, N.R. Tao, L. Lu, Anisotropic strengthening of nanotwin bundles in heterogeneous nanostructured Cu: Effect of deformation compatibility, Acta Mater. 210 (2021), 116830.
[9] A. Misra, J.P. Hirth, R.G. Hoagland, Length-scale-dependent deformation mechanisms in incoherent metallic multilayered composites, Acta Mater. 53 (18) (2005) 4817–4824.
[10] K. Lu, Stabilizing nanostructures in metals using grain and twin boundary architectures, Nat. Rev. Mater. 1 (5) (2016) 16019.
[11] F. Sansoz, K. Lu, T. Zhu, A. Misra, Strengthening and plasticity in nanotwinned metals, MRS Bull. 41 (4) (2016) 292–297.
[12] N. Li, J. Wang, A. Misra, X. Zhang, J.Y. Huang, J.P. Hirth, Twinning dislocation multiplication at a coherent twin boundary, Acta Mater. 59 (15) (2011) 5989–5996.
[13] Q. Lu, Z. You, X. Huang, N. Hansen, L. Lu, Dependence of dislocation structure on orientation and slip systems in highly oriented nanotwinned Cu, Acta Mater. 127 (2017) 85–97.
[14] Z.H. Jin, P. Gumbsch, E. Ma, K. Albe, K. Lu, H. Hahn, H. Gleiter, The interaction mechanism of screw dislocations with coherent twin boundaries in different face-centred cubic metals, Scr. Mater. 54 (6) (2006) 1163–1168.
[15] Z.X. Wu, Y.W. Zhang, D.J. Srolovitz, Dislocation–twin interaction mechanisms for ultrahigh strength and ductility in nanotwinned metals, Acta Mater. 57 (15) (2009) 4508–4518.
[16] Y.T. Zhu, X.Z. Liao, X.L. Wu, Deformation twinning in nanocrystalline materials, Prog. Mater. Sci. 57 (1) (2012) 1–62.
[17] I.J. Beyerlein, X. Zhang, A. Misra, Growth twins and deformation twins in metals, Annu. Rev. Mater. Res. 44 (1) (2014) 329–363.
[18] X. Feaugas, On the origin of the tensile flow stress in the stainless steel AISI 316L at 300 K: back stress and effective stress, Acta Mater. 47 (13) (1999) 3617–3632.
[19] D. Kuhlmann-Wilsdorf, C. Laird, Dislocation behavior in fatigue II. Friction stress and back stress as inferred from an analysis of hysteresis loops, Mater. Sci. Eng. 37 (2) (1979) 111–120.
[20] H. Mughrabi, Dislocation wall and cell structures and long-range internal-stresses in deformed metal crystals, Acta Metall. 31 (9) (1983) 1367–1379.
[21] J. Dickson, J. Boutin, L. Handfield, A comparison of two simple methods for measuring cyclic internal and effective stresses, Mater. Sci. Eng. 64 (1) (1984) L7–L11.
[22] Z. Cheng, L. Bu, Y. Zhang, H. Wu, T. Zhu, H. Gao, L. Lu, Unraveling the origin of extra strengthening in gradient nanotwinned metals, Proc. Natl. Acad. Sci. U. S. A. 119 (3) (2022), e2116808119.
[23] Z. You, X. Li, L. Gui, Q. Lu, T. Zhu, H. Gao, L. Lu, Plastic anisotropy and associated deformation mechanisms in nanotwinned metals, Acta Mater. 61 (1) (2013) 217–227.
[24] U. Kocks, H. Mecking, Physics and phenomenology of strain hardening: the FCC case, Prog. Mater. Sci. 48 (3) (2003) 171–273.
[25] J. Wang, A. Misra, An overview of interface-dominated deformation mechanisms in metallic multilayers, Curr. Opin. Solid State Mater. Sci. 15 (1) (2011) 20–28.
[26] Q. Zhu, L. Kong, H. Lu, Q. Huang, Y. Chen, Y. Liu, W. Yang, Z. Zhang, F. Sansoz, H. Zhou, J. Wang, Revealing extreme twin-boundary shear deformability in metallic nanocrystals, Sci. Adv. 7 (36) (2021) eabe4758.
[27] H. Zhou, X. Li, S. Qu, W. Yang, H. Gao, A jogged dislocation governed strengthening mechanism in nanotwinned metals, Nano Lett. 14 (9) (2014) 5075–5080.
[28] H. Zhou, H. Gao, A plastic deformation mechanism by necklace dislocations near crack-like defects in nanotwinned metals, J. Appl. Mech. 82 (7) (2015), 071015.
[29] Q. Pan, H. Zhou, Q. Lu, H. Gao, L. Lu, History-independent cyclic response of nanotwinned metals, Nature 551 (7679) (2017) 214–217.
[30] W.G. Hoover, Canonical dynamics: Equilibrium phase-space distributions, Phys. Rev. A 31 (3) (1985) 1695–1697.
[31] Y. Mishin, M.J. Mehl, D.A. Papaconstantopoulos, A.F. Voter, J.D. Kress, Structural stability and lattice defects in copper: *Ab initio*, tight-binding, and embedded-atom calculations, Phys. Rev. B 63 (22) (2001), 224106.
[32] A. Stukowski, Visualization and analysis of atomistic simulation data with OVITO–the open visualization tool, Modell. Simul. Mater. Sci. Eng. 18 (1) (2009), 015012.
[33] F.R.N. Nabarro, Cottrell-stokes law and activation theory, Acta Metall. Mater. 38 (2) (1990) 161–164.
[34] T. Zhu, J. Li, A. Samanta, H.G. Kim, S. Suresh, Interfacial plasticity governs strain rate sensitivity and ductility in nanostructured metals, Proc. Natl. Acad. Sci. U. S. A. 104 (9) (2007) 3031–3036.